Journal of Power Sources 242 (2013) 610–620

Contents lists available at SciVerse ScienceDirect

Journal of Power Sources

journal homepage: www.elsevier.com/locate/jpowsour

High activity of carbon nanotubes supported binary and ternary Pd-based catalysts for methanol, ethanol and formic acid electro-oxidation

Fuchun Zhu [a], Guanshui Ma [a], Zhongchao Bai [a], Ruiqiang Hang [a], Bin Tang [a], Zhonghua Zhang [b], Xiaoguang Wang [a,*]

[a] Research Institute of Surface Engineering, Taiyuan University of Technology, Yingze West Road 79, Taiyuan 030024, PR China
[b] Key Laboratory for Liquid-Solid Structural Evolution and Processing of Materials, Ministry of Education, Shandong University, Jingshi Road 17923, Jinan 250061, PR China

HIGHLIGHTS

- Pd-based bi-/ternary catalysts were synthesized with Sn or/and Cu as alloying element.
- PdCuSn/CNTs exhibits the highest activities for targeted molecules electro-oxidation.
- Activity enhancement may derive from distinct effect by alloying with Cu and Sn.
- Alloying of Sn is even more remarkable for ethanol and formic acid oxidation.

ARTICLE INFO

Article history:
Received 7 March 2013
Received in revised form
9 May 2013
Accepted 27 May 2013
Available online 5 June 2013

Keywords:
Palladium
Electrocatalyst
Multi-walled carbon nanotubes
Electro-oxidation
Methanol
Formic acid

ABSTRACT

In this study, we have synthesized a series of multi-walled carbon nanotubes supported Pd, PdCu(molar ratio 1:1), PdSn(1:1) and PdCuSn(1:1:1) catalysts by chemical reduction with $NaBH_4$ as a reducing agent. These catalysts are characterized using X-ray diffraction, transmission electron microscopy, energy dispersive X-ray spectroscopy, X-ray photoelectron spectroscopy (XPS), cyclic voltammetry and chronoamperometry. During the potential cycling activation, it is found that the additive Cu is prone to suffer leaching while the dissolution of Sn rarely occurs. Electrochemical measurements demonstrate that, the co-alloying of Pd with Cu and Sn can trigger the best catalytic activity enhancement as compared with the binary PdCu/CNTs, PdSn/CNTs and mono-component Pd/CNTs catalysts. The PdCuSn/CNTs reveals the most excellent activities toward methanol, ethanol and formic acid electro-oxidation and the corresponding mass activity can attain to 395.94, 872.70 and 534.83 mA mg^{-1} Pd, respectively. The possible promotion effect of additive Sn or/and Cu on the electrocatalytic activity improvement is also analyzed.

1. Introduction

Nowadays, great attention has been paid to direct alcohol fuel cells (DAFCs) and direct formic acid fuel cells (DFAFCs) in view of their great potential in green-energy technologies [1,2]. In research for new candidate for Pt-based catalysts, Pd has attracted much attention in recent years due to many advantages such as, being more cost-effective than Pt and having remarkable electrocatalytic activity toward some small organic molecules in alkaline and acidic circumstance [3,4]. In order to further improve the electrocatalytic performance of mono-Pd catalyst, most of the work has addressed to the modification of Pd environment by alloying with other elements or through the synthesis of multi-functional electrocatalysts [5–7]. Until now, the most successful results have been achieved through the alloying route. Commonly, the additive element used to alloying with Pd has been chosen under the condition that it should provide oxygen-containing species at low potentials to oxidize adsorbed CO, thereby decreasing catalytic poisoning, such as Ag [8], Bi [9], Ni [10,11], Co [12] and so forth. It should be worth noting that, the presence of a second additive transition metal not only has a significant impact on its activity and stability, but also

* Corresponding author. Tel./fax: +86 351 6010540.
E-mail addresses: wangxiaoguang@tyut.edu.cn, wangxiaog1982@163.com (X. Wang).

0378-7753/$ – see front matter © 2013 Elsevier B.V. All rights reserved.
http://dx.doi.org/10.1016/j.jpowsour.2013.05.145

can greatly reduce Pd loading so as to lower the usage of precious metals. Simultaneously, the appropriate selection of catalyst supporting material is also a key factor to reduce the noble metal loading and the system cost as well. Till now, different types of carbon supporting materials such as active carbon, multi-walled carbon nanotubes (MWCNTs), and graphite carbon nanofibers (GCNFs) have been widely reported [13–15]. Among them, carbon nanotubes (CNTs) are generally considered as attractive supporting material because of the nanometer size, high-accessible surface area and good electric conductivity, which can further improve the noble metal utilization and may trigger enhanced performance in fuel cell applications [16,17]. For example, previous studies reported that, carbon nanotubes-supported Pd-M (M = Ag [18], Co [19]) catalyst exhibits even better catalytic activity toward organic species as compared with the counterpart supported on common carbon black materials.

Recently, Xu et al. [20] synthesized several bimetallic nanoporous PdCu catalysts through dealloying of AlPdCu precursor and ascribed their superior activities for methanol and formic acid electro-oxidation to the synergistic interaction between Pd-skin and PdCu-core. By virtue of a similar methodology, Zhang et al. [21] also obtained a kind of ultra-fine nanoporous CuPd alloy nanostructures with ligaments/channels of less than 10 nm, which reveal superior electrocatalytic performance toward electro-oxidation of methanol and ethanol in alkaline media. Moreover, Liu et al. [22] and Tu et al. [23] reported that PdSn/C catalyst revealed an improved activity for formic acid electro-oxidation than Pd/C owing to the electronic effect induced by alloying of Sn. Apart from the initial alloying, however, a further electrochemical leaching or dissolution can selectively etch partial non-noble atoms away and the activity of alloy nanoparticle catalysts will reach a high level due to the enhanced short-range chemical ligand effects and/or long-range geometric effects such as lattice strain [24]. To date, Strasser and co-workers [25–30] systematically investigated the surface re-arrangement of Pt–M (M = Cu, Ni or/and Co) alloy nanoparticles when suffering an electrochemical cycling process and found that these electrochemically pretreated catalysts can acquire further improved activities toward oxygen reduction reaction as compared with the benchmark Pt/C catalyst.

Although either Cu or Sn is generally considered as an efficient alloying element with Pd to induce an enhanced catalytic performance, to our knowledge, little work is available for co-alloying of Cu and Sn together with Pd to generate a ternary PdCuSn catalyst supported on CNTs. Herein, we successfully synthesized a series of multi-walled CNTs-supported Pd and Pd-based bi-/ternary catalysts (Pd/CNTs, PdCu/CNTs, PdSn/CNTs and PdCuSn/CNTs) through borohydride reduction method. Additionally, the influence of alloying Sn or/and Cu on the potential redox activation behavior as well as the electrocatalytic activity enhancement for methanol, ethanol and formic acid electro-oxidation has been analyzed for the first time in this article. Based upon the co-operative effect of Cu and Sn additives as well as the induced superior catalytic activity and durability, the ternary PdCuSn/CNTs reveals great potential as less expensive anodic electrocatalyst in the applications of DAFCs and DFAFCs.

2. Experimental

2.1. Preparation of catalysts

The functionalization of multi-walled CNTs (Ø 50 nm, Shenzhen Nanotech Port Co. Ltd.) was performed in a concentrated HNO_3 (70%) at 80 °C for 2 h and then washed repeatedly with ultra-purified water and evaporated to dryness. Each single Pd/CNTs, binary PdCu(molar ratio 1:1)/CNTs, PdSn(1:1)/CNTs and ternary PdCuSn(1:1:1)/CNTs were synthesized using $PdCl_2$, $CuSO_4 \cdot 5H_2O$ and $SnCl_2 \cdot 2H_2O$ as metal sources, $NaBH_4$ as reducing agent and functionalized-CNTs as support. All the chemicals used were analytical grade. The required stoichiometric amount of metal source salts were dissolved in ethylene glycol, and then an appropriate amount of functionalized-CNTs (ca. 25 wt.% metal/75 wt.% CNTs) was added and ultrasonically stirred for 1 h. After that, a mixing solution of $NaBH_4$ and ethanol with a pH value of ca. 12 was added, drop by drop, to the well-dispersed mixtures under vigorous stirring to facilitate the decoration of metals on the CNTs surface. Finally, the as-obtained suspensions were washed several times to remove residual salts, centrifuged and dried.

2.2. Characterization of catalysts

X-ray diffraction (XRD) profiles were collected using a Bruker-D8-Advance X-ray diffractometer with Cu Kα radiation (λ = 0.15406 nm). The microstructure and chemical composition were analyzed using a transmission electron microscopy (TEM, JEM-2100) and an energy dispersive X-ray analyzer (EDX, Bruker-QX-200). X-ray photoelectron spectroscopy (XPS) spectra were recorded using a K-Alpha (Thermo Scientific ESCALAB 250) spectrometer equipped with monochromatic Al Kα radiation operating at 15 kV and 10 mA, and the binding energies (BE) were corrected by referencing the C1s peak to 284.8 eV.

2.3. Electrochemical measurements

All electrochemical measurements were conducted in a standard three-electrode cell using a CS-350 Potentiostat. The working electrode was prepared by thin-film electrode method as follows [31]: The catalyst of 5 mg was firstly ultrasonically mixed with 300 μL isopropanol and 100 μL Nafion solution (0.5 wt.%) to form a well-dispersed catalyst ink. Then, 5 μl of the ink obtained was pipetted and spread on a polished glassy carbon electrode (GCE, Ø 4 mm) as the working electrode. According to the stoichiometry of catalysts ink, the resulting homogenous catalytic film on the GC electrode surface obtained a calculated Pd loading of 124.3, 77.8, 58.8 and 45.8 μg(Pd) cm^{-2} for Pd/CNTs, PdCu/CNTs, PdSn/CNTs and PdCuSn/CNTs, respectively. The counter electrode was a bright Pt plate, and a saturated calomel electrode (SCE) or an Hg/HgO (1.0 M KOH) electrode (MMO) was used as the reference electrode, depending on the experimental requirements. The voltammetric activation behavior was characterized in a 0.5 M H_2SO_4 solution and corresponding electrocatalytic activities toward methanol, ethanol and formic acid oxidation were measured in the solutions of 1.0 M KOH + 0.5 M MeOH, 1.0 M KOH + 0.5 M EtOH and 0.5 M H_2SO_4 + 0.5 M HCOOH, respectively. The current densities were normalized by equivalent mass of Pd on the GCE surface. Before tests, the electrolytes were de-oxygenated by bubbling N_2 for 30 min. All electrochemical experiments were performed at ambient temperature (~25 °C).

3. Results and discussion

3.1. Physical characterization of Pd and Pd-based catalysts

Fig. 1 shows the XRD profiles of Pd/CNTs, PdCu/CNTs, PdSn/CNTs and PdCuSn/CNTs catalysts. For all the samples, the broad peak at about 25° is associated with the (002) plane of multi-walled CNTs [32]. The peaks around 39.9°, 46.3° and 67.9° can be attributed to the diffraction peaks of Pd crystal faces (111), (200) and (220), indicating these catalysts have prevailed face-centered cubic (fcc) Pd structure. For the PdCu and PdCuSn catalyst, a tiny diffraction peak located at ca. 23° should derive from the (021) plane of a trace amount of $Cu(OH)_2$, which may also be easily formed at high pH

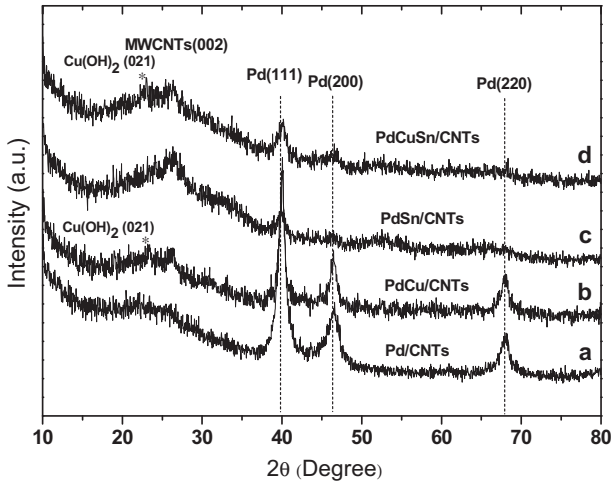

Fig. 1. XRD patterns of the (a) Pd/CNTs, (b) PdCu/CNTs, (c) PdSn/CNTs and (d) PdCuSn/CNTs catalysts.

value [33,34]. No diffraction peaks, which indicate the presence of either pure Cu and Sn metals, appear in the XRD patterns, suggesting that Cu and Sn atoms either form an alloy with Pd or exist as oxides in amorphous phase. It should be mentioned that the emergence of one set of fcc diffraction peaks can also be found in the commonly-reported bi-/ternary Pd- or Pt-based alloy catalysts, such as Pd–Ni [16,22], Pd–Co [19], Pd–Pb [35], Pd–Ag [18], Pt–Sn [36], Pt–Ni–Pb [37], Pt–Sn–Rh [38], and so forth. Relative to the mono-Pd (marked with the vertical dashed lines), the diffraction peaks for PdCu are shifted slightly to higher 2θ values due to the incorporation of smaller Cu atoms into the fcc structure of Pd [20]. Whereas, the diffraction peaks for PdSn are shifted to lower 2θ values and consistent with the fact that the addition of Sn can increase the lattice parameter of Pd crystals [22]. The d spacings of (111) peaks can be calculated via the Bragg law:

$$d = \frac{\lambda}{2\sin\theta} \tag{1}$$

where λ is the X-ray wavelength ($\lambda = 1.5418$ Å) and θ is the angle of (111) peaks. And the lattice parameter (a) of the catalysts can also be obtained based upon the following equation:

$$d_{111} = \frac{a}{\sqrt{1^2 + 1^2 + 1^2}} \tag{2}$$

Additionally, the average particle size (L) may be estimated according to Debye-Scherrer formula [39]:

$$L = \frac{0.9\lambda}{B_{2\theta}\cos\theta} \tag{3}$$

where L is the mean size of particles (nm), λ is the wavelength of X-ray ($\lambda = 1.5418$ Å), θ is the angle of (111) peak, and $B_{2\theta}$ is the width (in radians) of (111) peak at half height. The calculated lattice parameter and average particle size of these as-synthesized catalysts were summarized in Table 1. It can be found that lattice parameter of the catalysts follows the order: PdSn (3.928 Å) > Pd (3.910 Å) > PdCuSn (3.898 Å) > PdCu (3.889 Å). And the average particle size follows the sequence: PdCu (15.1 nm) > Pd (10.5 nm) > PdSn (8.1 nm) > PdCuSn (7.1 nm). Obviously, the incorporation of Sn into Pd significantly diminishes the average particle size of the catalyst. As for the Sn-related sample, such as PdSn and PdCuSn, it is intriguing that the (220) plane almost cannot be detected. The resulted larger $B_{2\theta}$ value by the incorporation of Sn coupled with the possible induced low crystalline state may contribute to this phenomenon. Of course, the weakening of (220) plane can also be observed in several other widely-reported alloy catalysts, such as PdBi [9], PdCo [40], PtRuSn [41], PtRuP [42], etc.

Table 1
The XRD analysis of as-synthesized Pd/CNTs, PdCu/CNTs, PdSn/CNTs and PdCuSn/CNTs catalysts.

Catalyst	Pd (111) at 2θ/(°)	$d_{(111)}$/(Å)	Lattice parameter/(Å)	$B_{2\theta}$/(10^{-2} rad)	Crystallite size/(nm)
Pd/CNTs	39.90	2.258	3.910	1.395	10.5
PdCu/CNTs	40.13	2.245	3.889	0.977	15.1
PdSn/CNTs	39.71	2.268	3.928	1.814	8.1
PdCuSn/CNTs	40.03	2.251	3.898	2.076	7.1

Fig. 2 shows the morphology of as-functionalized MWCNTs support before metal modification. The bare MWCNTs reveal a smooth surface and the mean diameter of MWCNTs is located at ~50 nm. Moreover, most MWCNTs are isolated and nearly no agglomeration is observed. Fig. 3 shows typical TEM micrographs of the as-synthesized Pd/CNTs, PdCu/CNTs, PdSn/CNTs and PdCuSn/CNTs catalyst. As compared with the bare support, it is clear that metallic nanoparticles have been successfully decorated on the surface of MWCNTs. In addition, the mono-Pd metallic nanoparticles on the Pd/CNTs catalyst appear obvious agglomeration and some particles are even immerged together to form clumps (ca. 100 nm, marked with a black arrow) (Fig. 3a). In comparison, the dispersion of nanoparticles in the bi-/ternary catalysts exhibits more uniform as compared with the mono-Pd counterpart (Fig. 3b–d). Although there still exist some agglomerations, most of the metal nanoparticles exhibit an average size below 10 nm in the Sn-incorporated catalysts, such as PdSn/CNTs and PdCuSn/CNTs, which is in good agreement with that calculated from the XRD result. Previous study also reveals that a portion of Sn additive can contribute to a well-dispersion of metallic nanoparticles in the PdSn/C catalysts [23]. Chemical composition of the as-synthesized bi-/ternary catalysts was determined using EDX and the typical spectra are present in Fig. 4. The compositional values of these as-prepared catalysts were analyzed and illustrated in Table 2. It is obvious that the actual composition is quite similar to the nominal value.

3.2. Cyclic voltammogram behavior and evaluation of electrochemically active surface area

In general, conducting a pre-positive potential cycling can not only clean the catalyst surface to improve its reactivity but also

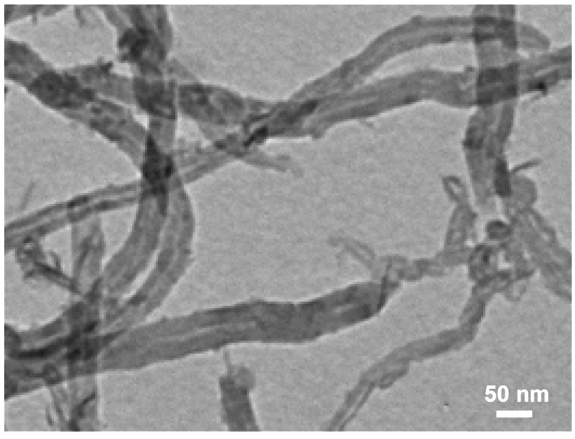

Fig. 2. TEM image of the as-functionalized multi-walled CNTs.

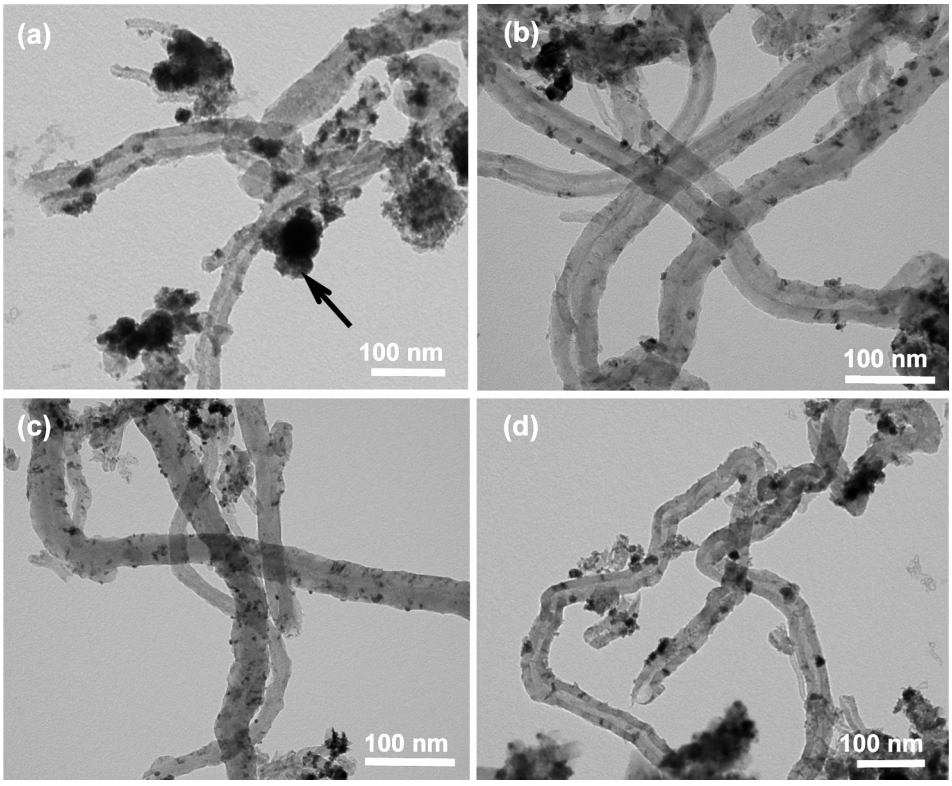

Fig. 3. TEM images of the (a) Pd/CNTs, (b) PdCu/CNTs, (c) PdSn/CNTs and (d) PdCuSn/CNTs catalysts.

represent the important electrochemical features, such as the typical underpotentially deposited hydrogen ad/desorption, double layer and metallic redox region [43,44]. Especially, for some typical bi-/ternary metallic nanoparticle catalysts, such as PtCu and PtCo, the potential cycling can even induce the leaching of less-noble-metals (i.e. Cu and Co) in an acidic circumstance and contribute to the formation of a core–shell nanoparticle structure [25,29,30]. Also, the noble metals in these activated bi-/ternary catalysts should acquire more efficient utilization. Hence, a similar voltammetric pretreatment (or activation) has been performed on these as-prepared Pd-M (M = Cu or/and Sn) catalysts prior to the activity measurement.

Fig. 5 shows the successive cyclic voltammetry (CV) curves of Pd/CNTs, PdCu/CNTs, PdSn/CNTs and PdCuSn/CNTs in the 0.5 M H_2SO_4 solution. It is clear that, the curves of Pd/CNTs quickly reach a stable state and exhibit a typical profile same as mono-Pd nano-catalyst, comprising hydrogen adsorption/desorption, thin double layer charging and metallic redox region (Fig. 5a). For PdCu/CNTs, however, huge Cu dissolution peaks (peak 1 and 2) between −0.1 and 0.5 V were observed with the potential sweeping anodically in the first scan (Fig. 5b). In the subsequent scans, the dissolution peak 1 near 0.04 V disappeared completely, indicating a limited amount of un-alloyed Cu in the surface. The broad dissolution peak 2 at 0.26 V associated with Cu striping gradually decreased in intensity while H ad/desorption feature gradually emerged. The final CV of PdCu/CNTs strongly resembled that of mono-Pd, suggesting nearly no residual Cu in the surface. It can be found that the voltammetric leaching phenomenon of Cu in PdCu/CNTs is well consistent with that observed in PtCu/C, as reported by Strasser's group [45–47]. In comparison, the final time-stable profile of PdSn/CNTs exhibits no drastic change as compared with the initial curve (Fig. 5c), implying that Sn is hard to suffer depletion from the surface. Moreover, the existence of oxophilic Sn atoms on the PdSn/CNTs surface may be responsible for its thick double layer charging. As for the ternary PdCuSn/CNTs (Fig. 5d), the magnitude of representative signals referring to the dissolution of Cu (marked with a vertical arrow) was smaller than that of PdCu/CNTs. It is reasonable to assume that the co-existence of surrounded Sn atoms severely diminish the exposed Cu atoms on the surface so that the formation of leaching channels can be prohibited to some extent. And thus, the dissolution of Cu from PdCuSn nanoparticles could mainly occur in the surface rather than in the inner part. Accordingly, the final CV of PdCuSn/CNTs was in large part identical to that of PdSn/CNTs owing to the reason that only the Cu in the superficial surface was almost leached away while most of the Sn atoms were remained to generate a PdSn-rich skin.

In order to clarify the compositional change during the CV pre-activation process, the final bulk composition of the PdCu/CNTs, PdSn/CNTs and PdCuSn/CNTs catalyst with a stable voltammetric profile was also determined by EDX and the results are shown in Fig. 6 and Table 2. It is surprising that, most of the Cu has been leached away from the PdCu/CNTs when sweeping continuous potential cycling to the stable state. Similarly, Mani and Strasser [48] also reported that, successive electrochemical voltage cycling can change the bulk compositional ratio of Pt–Cu nanoparticles from $Pt_{25}Cu_{75}$ to $Pt_{87}Cu_{13}$ in 1.0 M H_2SO_4 solution. Distinct from the severe loss of Cu, however, only a tiny amount of Sn can be removed from PdSn/CNTs, which is also in line with that revealed by the CV results. In addition, the final composition of activated PdCuSn/CNTs further verifies that the addition of Sn can significantly hinder the Cu dissolution so that the leaching reaction may merely occur within the top-layer of the nanoparticles, which will be further depicted using XPS in the next part. Despite the compositional changes in the activated samples, the original atomic content will still be denoted in the following sections.

As is known to all, the oxygen adsorption/desorption method is usually applicable to evaluate the electrochemically active surface

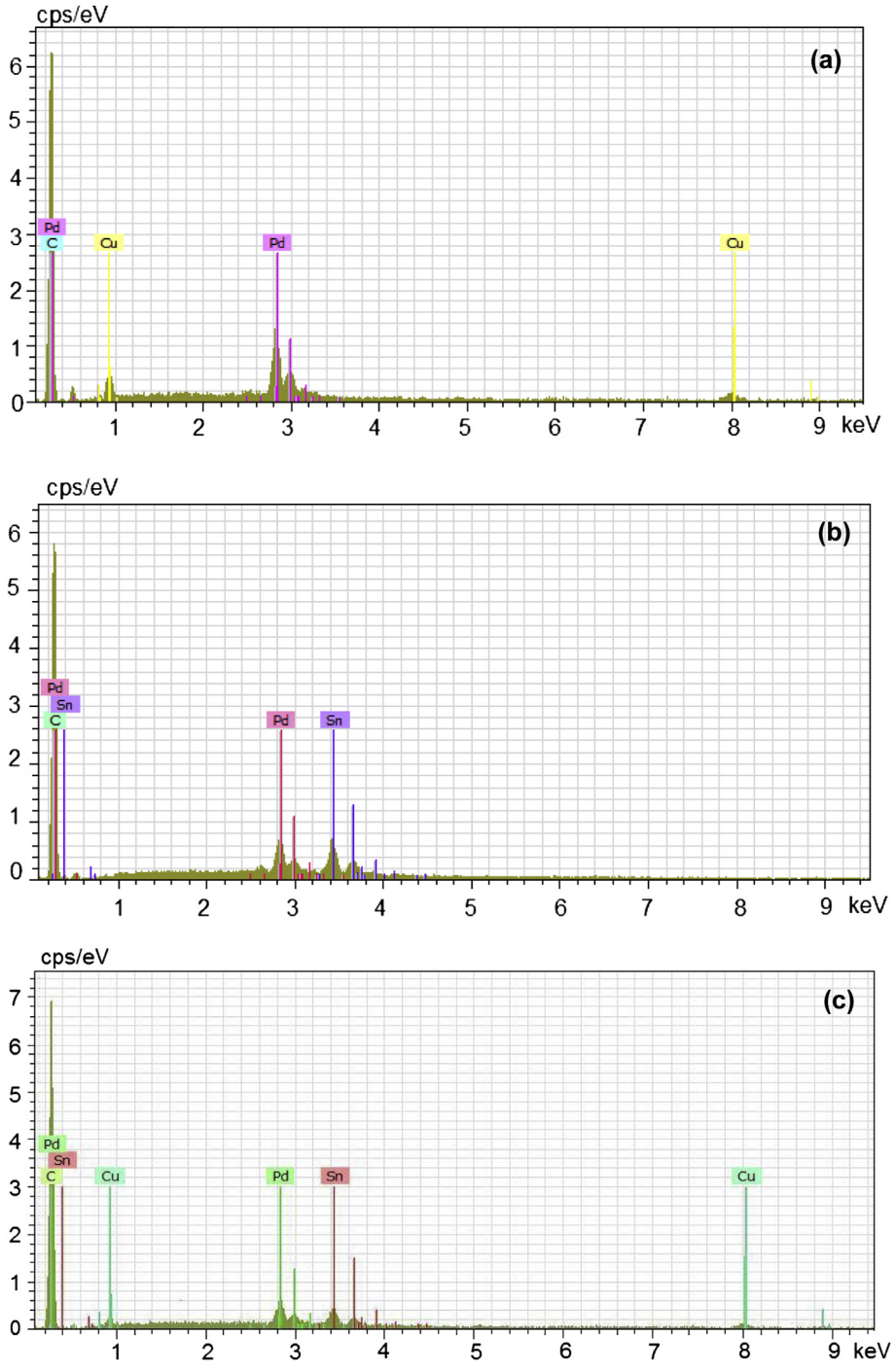

Fig. 4. Typical EDX spectra of the (a) PdCu/CNTs, (b) PdSn/CNTs and (c) PdCuSn/CNTs catalysts.

Table 2
The atomic composition of as-synthesized and activated bi-/ternary PdCu/CNTs, PdSn/CNTs and PdCuSn/CNTs catalysts.

Catalyst		Composition (at.%)		
		Pd	Cu	Sn
PdCu/CNTs	As-prepared	47.91	52.09	–
	Activated	92.91	7.09	–
PdSn/CNTs	As-prepared	43.41	–	56.59
	Activated	56.70	–	43.30
PdCuSn/CNTs	As-prepared	31.81	37.30	30.89
	Activated	47.29	20.82	31.89

areas (S_{EAS}) of the metals showing well-developed regions for oxide monolayer formation and reduction, such as Pd and Au [49]. Generally, the S_{EAS} of Pd or Pd-based catalysts can be estimated according to the following equation [44]:

$$S_{EAS} = \frac{Q_S}{Q_C \cdot m} \cdot 10^{-4} \quad (4)$$

where Q_S is the coulombic charge (in μC) determined by integrating current peak of Pd oxide reduction, Q_C is the conversion factor and has been commonly taken as 424 μC cm^{-2} corresponding to PdO reduction, and m is the loadings of Pd metal (mg) on the GC surface.

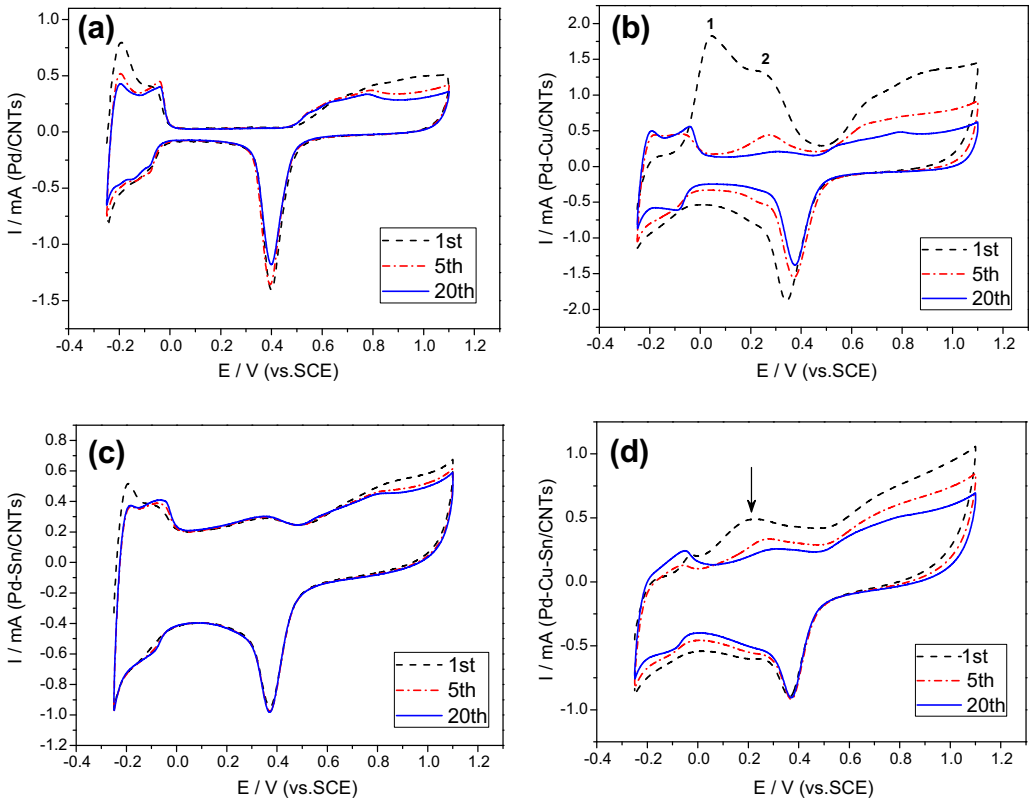

Fig. 5. Successive CV curves of the (a) Pd/CNTs (b) PdCu/CNTs (c) PdSn/CNTs and (d) PdCuSn/CNTs catalysts in the 0.5 M H_2SO_4 solution. Scan rate: 50 mV s^{-1}.

From the stable voltammetric profiles, the S_{EAS} of the catalysts follows the sequence: PdCu/CNTs (39.07 m^2 g^{-1} Pd) > PdCuSn/CNTs (37.92 m^2 g^{-1} Pd) > PdSn/CNTs (25.94 m^2 g^{-1} Pd) > Pd/CNTs (19.64 m^2 g^{-1} Pd). Normally, the S_{EAS} of as-treated PtCu nanoparticles through voltage cycling treatment can range from ca. 21–72 m^2 g^{-1} Pt [48]. Zhao et al. [50] also reported that, the as-synthesized Pd/MWCNTs exhibits a S_{EAS} value of ca. 21.55 m^2 g^{-1} Pd. Obviously, the activated catalysts in the present study depict a comparable S_{EAS} value relative to those of as-reported Pt- and Pd-based counterparts. Meanwhile, it is noticed that the Cu-incorporated catalysts, such as PdCu/CNTs and PdCuSn/CNTs, exhibit a larger S_{EAS} value. We assume that it may derive from the re-arrangement of the superficial structure based upon the stripping of Cu atoms, which will contribute to the collapse of large particle as well as the exposure of large quantities of inner active Pd sites or underneath as well. Previous research also depicted that, potential cycling activation brings on the emergence of nanopores with sizes ranging from ~1 to ~5 nm throughout the $PdCu_6$ nanoparticles as well as the leaching away of about 85% Cu atoms [51]. Although the stable PdCu/CNTs exhibits the highest S_{EAS} value, it is interesting that a slightly decreased reduction peak area can also be observed with the successive potential cycling, which is consistent with that revealed in the potential cycling of PtCu [45,46]. As for this phenomenon, Cui et al. [52] reported that, the initial potential cycling would result in a Pt skeleton with a higher surface area. Following the successive cycling, the Pt skeleton would suffer both Ostwald ripening and coalescence to reach a more stable rough shell surface. Obviously, the change from the initial skeleton to rough stable shell could induce a certain loss of surface area but can contribute to a more stable surface topography. For the PdCu-related sample, it should rely on a similar mechanism as that of PtCu counterpart mentioned above. As for the PdSn/CNTs, the smaller average particle size should be the main causation for its larger S_{EAS} value than Pd/CNTs because almost no depletion of surface Sn atoms occurs.

3.3. Electrocatalytic activities for methanol and ethanol electro-oxidation in alkaline media

The electro-oxidation of methanol in alkaline media can be rationally described as follows [53,54]:

$$M + (CH_3OH) \leftrightarrow M\text{-}(CH_3OH)_{ads} \quad (5)$$

$$M\text{-}(CH_3OH)_{ads} + OH^- \rightarrow M\text{-}(CH_3O)_{ads} + H_2O + e^- \quad (6)$$

$$M\text{-}(CH_3O)_{ads} + OH^- \rightarrow M\text{-}(CH_2O)_{ads} + H_2O + e^- \quad (7)$$

$$M\text{-}(CH_2O)_{ads} + OH^- \rightarrow M\text{-}(CHO)_{ads} + H_2O + e^- \quad (8)$$

$$M\text{-}(CHO)_{ads} + OH^- \rightarrow M\text{-}(CO)_{ads} + H_2O + e^- \quad (9)$$

$$M\text{-}(CO)_{ads} + OH^- \rightarrow M\text{-}(COOH)_{ads} + e^- \quad (10)$$

$$M\text{-}(COOH)_{ads} + OH^- \rightarrow M + CO_2 + H_2O + e^- \quad (11)$$

In presence of adequate hydroxyl ions, the oxidation of M-$(CHO)_{ads}$ and M-$(CO)_{ads}$ may proceed directly through the following steps:

$$M\text{-}(CHO)_{ads} + 3OH^- \rightarrow M + CO_2 + 2H_2O + 3e^- \quad (12)$$

$$M\text{-}(CO)_{ads} + 2OH^- \rightarrow M + CO_2 + H_2O + 2e^- \quad (13)$$

Among the reaction steps mentioned, the involved several intermediate organic species have been identified by FTIR

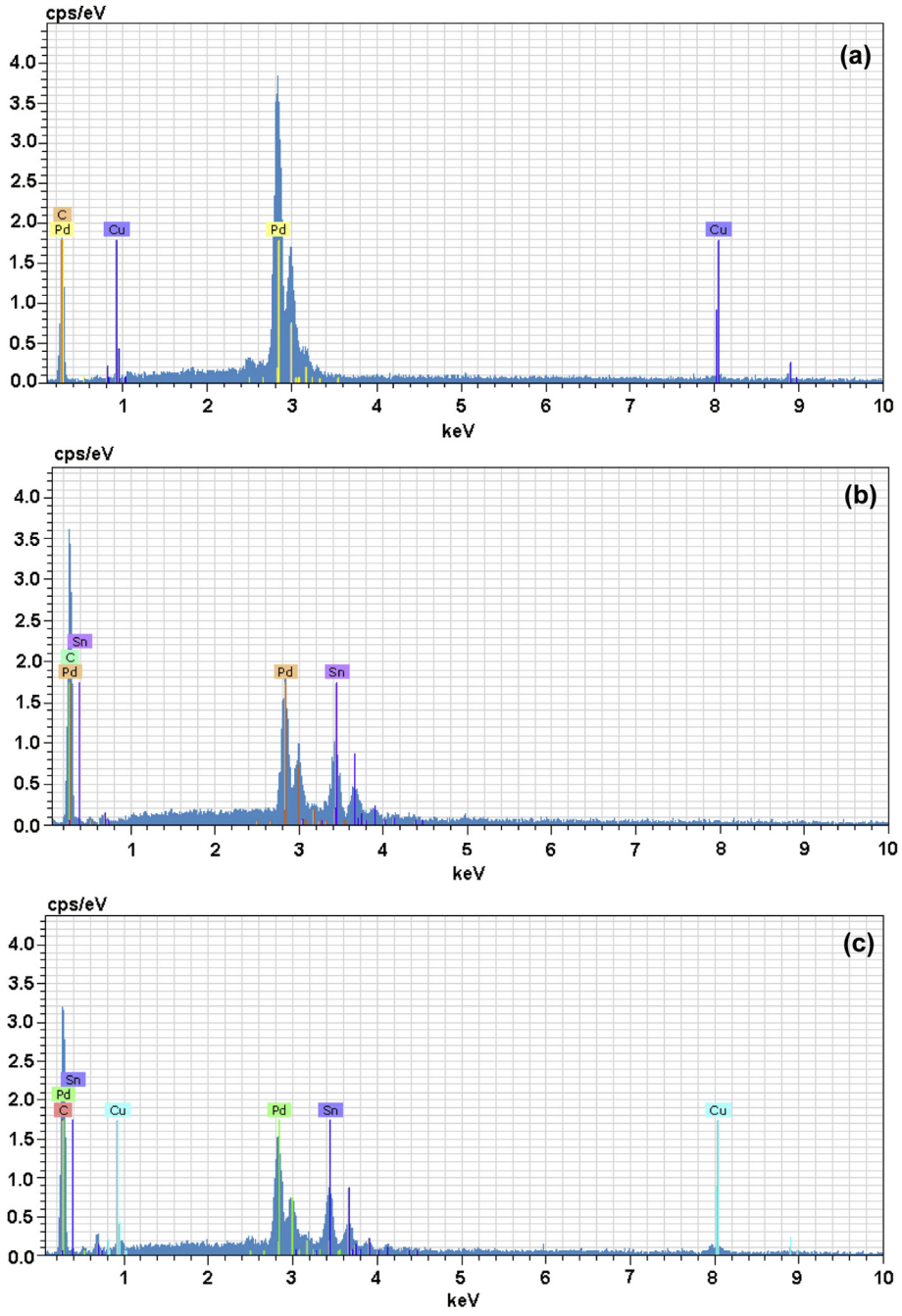

Fig. 6. Typical EDX spectra of the electrochemically activated (a) PdCu/CNTs, (b) PdSn/CNTs and (c) PdCuSn/CNTs catalysts.

spectroscopic study which revealed that the CO species are found to be linearly bonded to Pt sites (PtCO) and bridge bonded to Pd sites (Pd_2CO) [54]. Similarly, the electro-oxidation of ethanol takes place via the adsorption of ethanol molecule on active sites followed by reaction with hydroxyl ions to produce CH_3COOH, which exists in the form of CH_3COO^- ions in alkaline solution [55,56]:

$$M + CH_3CH_2OH \leftrightarrow M\text{-}(CH_3CH_2OH)_{ads} \quad (14)$$

$$M\text{-}(CH_3CH_2OH)_{ads} + 3OH^- \rightarrow M\text{-}(CH_3CO)_{ads} + 3H_2O + 3e^- \quad (15)$$

$$M + OH^- \leftrightarrow M\text{-}OH_{ads} + e^- \quad (16)$$

$$M\text{-}(CH_3CO)_{ads} + M\text{-}OH_{ads} \rightarrow M\text{-}CH_3COOH + M \quad (17)$$

$$M\text{-}CH_3COOH + OH^- \rightarrow M + CH_3COO^- + H_2O \quad (18)$$

To evaluate the activities toward methanol and ethanol electro-oxidation, the CVs of Pd/CNTs, PdCu/CNTs, PdSn/CNTs and PdCuSn/CNTs were performed in solutions of 1.0 M KOH + 0.5 M MeOH and 1.0 M KOH + 0.5 M EtOH, respectively. It is clear that the electrochemical oxidation of methanol and ethanol on the Pd and Pd-based catalysts was characterized by two well-defined current peaks on the forward and reverse scans, as illustrated in Figs. 7a and 8a. In the forward scan, the oxidation peak is correlated with the oxidation of freshly chemisorbed species which come from alcohol adsorption, and is normally used to evaluate the catalytic activity of electrocatalysts [57,58]. The reverse scan peak is primarily associated with the removal of carbonaceous species which

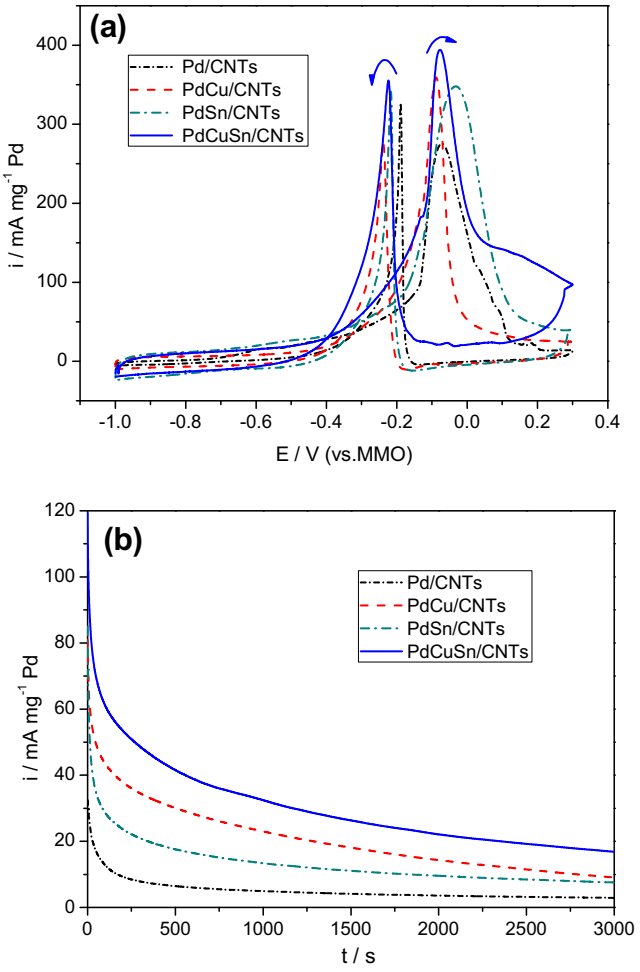

Fig. 7. (a) CV curves of the activated Pd/CNTs, PdCu/CNTs, PdSn/CNTs and PdCuSn/CNTs catalysts in the N_2 saturated solution of 1.0 M KOH + 0.5 M MeOH. Scan rate: 50 mV s^{-1}. (b) CA curves of the catalysts in solution of 1.0 M KOH + 0.5 M MeOH at a fixed potential of −100 mV (vs. MMO).

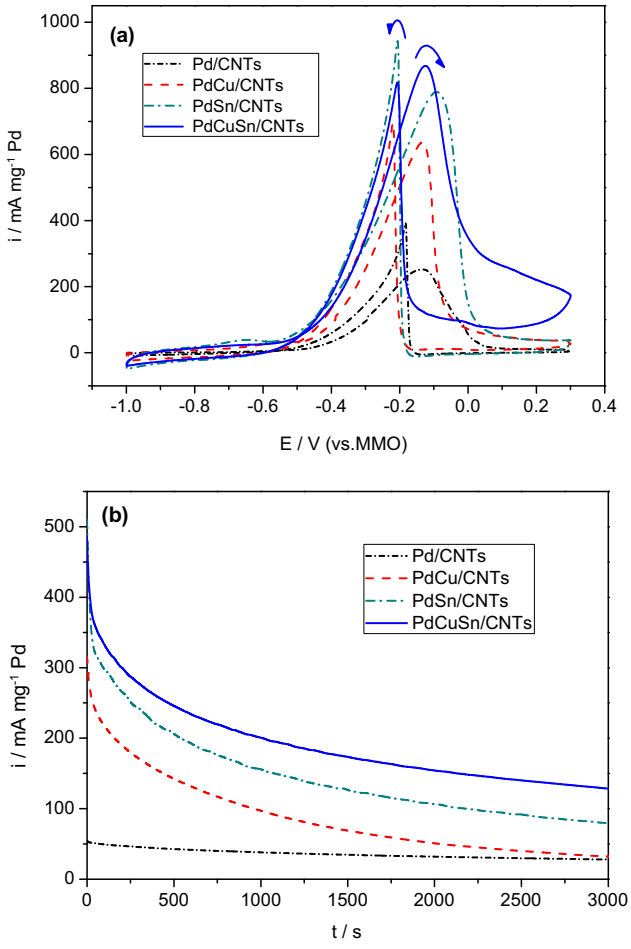

Fig. 8. (a) CV curves of the activated Pd/CNTs, PdCu/CNTs, PdSn/CNTs and PdCuSn/CNTs catalysts in the N_2 saturated solution of 1.0 M KOH + 0.5 M EtOH. Scan rate: 50 mV s^{-1}. (b) CA curves of the catalysts in solution of 1.0 M KOH + 0.5 M EtOH at a fixed potential of −200 mV (vs. MMO).

are not completely oxidized in the forward scan [59,60]. The onset oxidation potential, peak potential and mass normalized current density for the forward scan were analyzed and their values are shown in Tables 3 and 4 corresponding to the electro-oxidation of methanol and ethanol, respectively.

For both methanol and ethanol oxidation, it is clear that the activity of mono-Pd catalyst can be promoted by the incorporation of Cu or/and Sn, which is consistent with those of previous studies [20–23]. It can also be found that the activity enhancement induced by alloying with Cu or/and Sn is more prominent in ethanol oxidation than that in methanol oxidation. In the case of methanol oxidation, however, the promotion effect of Sn (with a promotion ratio of ca. 128) is almost comparable with that of Cu (with a promotion ratio of ca. 131). In comparison, there exists a significant promotion effect of Sn (with a promotion ratio of ca. 311) than that of Cu (with a promotion ratio of ca. 251) in the ethanol oxidation, indicating that Sn could act as a more efficient promoter in this case. Among the catalysts investigated, it is clear that the PdCuSn/CNTs exhibits the highest activities for both methanol and ethanol electro-oxidation and the values of mass activity can attain to 395.94 and 872.70 mA mg^{-1} Pd, respectively. Zhao et al. [50] reported that, Pd/Vulcan, Pd/MWCNTs and Pd–MnO_2/MWCNTs catalyst can reach the activities of 200, 275 and 425 mA mg^{-1} Pd by conducting the cyclic voltammograms in alkaline solutions containing 1.0 M methanol at a potential scan rate of 50 mV s^{-1}. In despite of only applying half of the methanol concentration, it can be observed that the activity of PdCuSn/CNTs catalyst is even comparable with that of MnO_2-promoted composite catalyst. As for the ethanol oxidation, Neto et al. [9] claimed that, PdBi(95:5)/C catalyst merely reach an activity of ca. 58 mA mg^{-1} Pd when performing cyclic voltammograms in 1.0 M KOH + 1.0 M ethanol. Hu et al. [61] synthesized a kind of Pd/TiO_2 composite catalyst with carbonized TiO_2 nanotubes as the support and a specific mass activity of ca. 270 mA mg^{-1} Pd can be obtained. In addition, Zhu et al. [62] depicted that, ethanol electro-oxidation reaction on Pd/C, Pd@Au(1:1)/C, Pd@Au(1:4)/C and Pd@Au(1:6)/C in solution of 1.0 M KOH + 1.0 M ethanol can contribute to a mass normalized activity of 135, 340, 796 and 405 mA mg^{-1} Pd, respectively. In our previous work, we also developed a novel Raney-like nanoporous Pd catalyst

Table 3
Cyclic voltammogram parameters for methanol oxidation on different electrodes in the electrolyte of 1.0 M KOH + 0.5 M MeOH.

Catalyst	Onset potential/ (mV vs. MMO)	Peak potential/ (mV vs. MMO)	Mass activity/ (mA mg^{-1} Pd)	Promotion ratio (%)
Pd/CNTs	−455	−69	274.49	100
PdCu/CNTs	−472	−88	360.42	131
PdSn/CNTs	−467	−33	350.03	128
PdCuSn/CNTs	−478	−78	395.94	144

Table 4
Cyclic voltammogram parameters for ethanol oxidation on different electrodes in the electrolyte of 1.0 M KOH + 0.5 M EtOH.

Catalyst	Onset potential/ (mV vs. MMO)	Peak potential/ (mV vs. MMO)	Mass activity/ (mA mg^{-1} Pd)	Promotion ratio (%)
Pd/CNTs	−448	−131	254.91	100
PdCu/CNTs	−486	−131	639.86	251
PdSn/CNTs	−577	−89	791.97	311
PdCuSn/CNTs	−583	−131	872.70	342

with superior electrocatalytic activity as high as ca. 300 mA mg^{-1} Pd toward ethanol oxidation in alkaline circumstance [63]. Obviously, the PdCuSn/CNTs catalyst is still competitive as compared with those of widely-reported metallic and composite nanocatalysts. Meanwhile, the onset potential of methanol and ethanol electro-oxidation on PdCuSn/CNTs shifts to a more negative value as compared with that on PdCu/CNTs, PdSn/CNTs and Pd/CNTs. It indicates that the kinetics of electrocatalytic reactions can be significantly enhanced on the PdCuSn/CNTs, which is important for its application in fuel cells. Moreover, further evaluation for catalytic durability of the electrocatalysts was conducted by chronoamperometry (CA) (Figs. 7b and 8b). All the as-doped catalysts depict a relatively good durability in the targeted time-scale, and should contribute to the reason that the additional transition elements minimize the accumulation of poisoning species on the active site so as to enhance the main oxidation reactions. As expected, the PdCuSn/CNTs demonstrates the highest current densities in the test period and the stability sequence of the catalysts for methanol and ethanol oxidation is in good agreement with the CV results.

3.4. Electrocatalytic activities for formic acid electro-oxidation in acidic media

Formic acid is also a potential fuel of interest for fuel cell applications. Unlike ethanol, however, C–C bond cleavage is not necessary, nor does additional oxygen need to be provided to generate CO_2, as would be the case for both methanol and ethanol [64]. Thus, it is believed that any electrode that is active for either methanol or ethanol should also show pronounced activity for formic acid. It is known that formic acid oxidation can progress through two parallel pathways: a “direct path way” in which formic acid is oxidized directly into CO_2 and a “CO path way”, which goes through the CO intermediate [65,66]. In the case of Pd-containing catalysts, formic acid oxidation occurs on Pd sites through the direct path way [67,68]. Firstly, formic acid is adsorbed onto the catalyst surface to form adsorptive formate:

$$HCOOH \rightarrow COOH_{ads} + H^+ + e^- \quad (19)$$

And then, the electro-oxidation reaction follows the reaction path:

$$COOH_{ads} \rightarrow CO_2 + H^+ + e^- \text{ (dehydrogenation)} \quad (20)$$

Here, the activities of the catalysts toward formic acid electro-oxidation were also examined, as shown in Fig. 9 and Table 5. It is clear that the current peaks referring to formic acid oxidation reaction are located in the same potential range in both forward and backward scan, further indicating that a dehydrogenation mechanism occurs overwhelmingly. Moreover, a notable activity enhancement can be observed when alloying Pd with Cu or/and Sn. The activity of the catalyst for formic acid oxidation reveals the same sequence as that for ethanol oxidation, and follows:

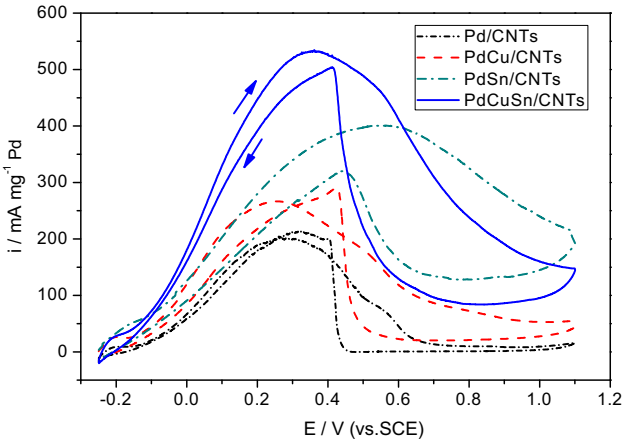

Fig. 9. CV curves of the activated Pd/CNTs, PdCu/CNTs, PdSn/CNTs and PdCuSn/CNTs catalysts in the N_2 saturated solution of 0.5 M H_2SO_4 + 0.5 M HCOOH. Scan rate: 50 mV s^{-1}.

PdCuSn/CNTs (534.83 mA mg^{-1} Pd) > PdSn/CNTs (401.40 mA mg^{-1} Pd) > PdCu/CNTs (267.97 mA mg^{-1} Pd) > Pd/CNTs (200.07 mA mg^{-1} Pd). Obviously, the promotion effect of Sn (with a promotion ratio of ca. 201) for formic acid oxidation is more remarkable relative to that of Cu (with a promotion ratio of ca. 134). Similarly, it is observable that the onset potentials of formic acid electro-oxidation shift toward more negative directions when incorporating Cu or/and Sn into Pd catalyst. According to the investigation by Liu et al. [22], the activity of PdSn-related catalysts, such as Pd4Sn1/C, Pd3Sn1/C, Pd2Sn1/C and Pd1Sn1/C, can reach a level of 213, 225, 330 and 329 mA mg^{-1} Pd while the Pd/C catalyst can merely attain to 185 mA mg^{-1} Pd. It is also noticed that a comparable atomic ratio between Pd and alloying additive Sn can bring on the promising activity enhancement. It is generally recognized that the addition of Sn to Pd can weaken the adsorptive bond of generated intermediates, such as CO_{ads} and $COOH_{ads}$, and the neighboring Sn atoms can prevent the accumulation of poisoning-intermediates and more active Pd sites were available for the direct HCOOH decomposition via the direct path way to CO_2. This may explain why the PdSn/CNTs and PdCuSn/CNTs exhibit a superior activity for formic acid oxidation.

3.5. Possible enhancement mechanism of Cu and Sn additive in the PdCuSn/CNTs catalyst

Among the catalysts investigated, the PdCuSn/CNTs reveals the highest mass normalized activity for the oxidation of methanol, ethanol and formic acid. Obviously, the co-alloying of Cu and Sn together with Pd should be responsible for this exciting situation. From the CV result mentioned above, the Cu is prone to suffer stripping from the surface of catalyst during the activation process while the dissolution of Sn can rarely occur. This situation is also well consistent with that revealed by the XPS results. As shown in

Table 5
Cyclic voltammogram parameters for formic acid oxidation on different electrodes in the electrolyte of 0.5 M H_2SO_4 + 0.5 M HCOOH.

Catalyst	Onset potential/ (mV vs. SCE)	Peak potential/ (mV vs. SCE)	Mass activity/ (mA mg^{-1} Pd)	Promotion ratio (%)
Pd/CNTs	−149	260	200.07	100
PdCu/CNTs	−153	252	267.97	134
PdSn/CNTs	−153	548	401.40	201
PdCuSn/CNTs	−158	355	534.83	267

Fig. 10a, it is clear that the signal referring to Cu species is present in the near surface of the initial as-prepared PdCuSn/CNTs but almost cannot be detected in the voltage-cycled (activated) sample (highlighted by dashed rectangles). For clarity, the XPS spectra of Cu 2p regions of as-prepared and activated PdCuSn/CNTs catalysts are also given in Fig. 10b. If only the Pd3d, Cu2p and Sn3d are concerned, the near surface composition is ca. 29 at.% Pd, 39 at.% Cu and 32 at.% Sn for the as-prepared PdCuSn/CNTs while the relative

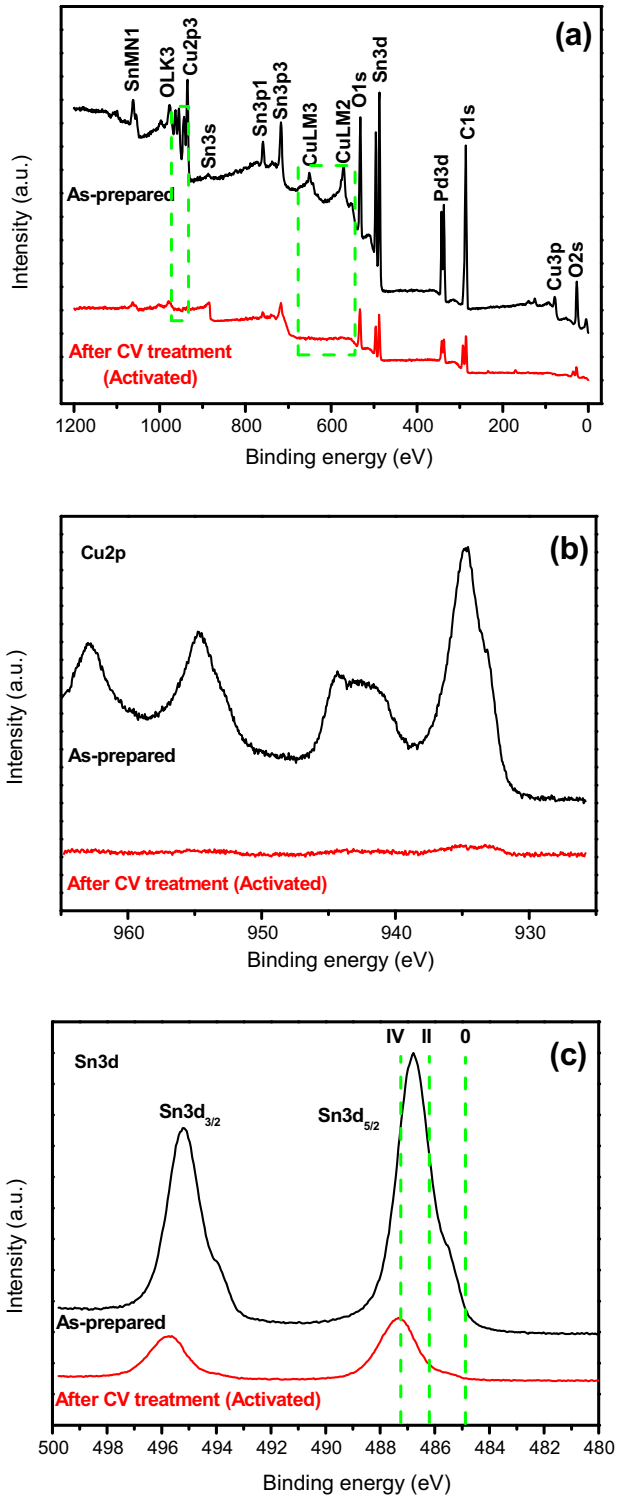

Fig. 10. XPS spectra of the as-synthesized and activated PdCuSn/CNTs catalyst. (a) full scan, (b) Cu 2p region and (c) Sn 3d region.

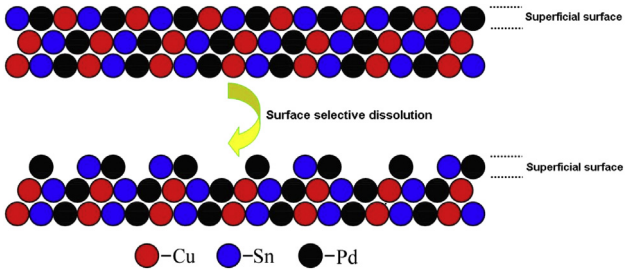

Fig. 11. Schematic surface atomic evolution of PdCuSn nanoparticles.

value is 53 at.% Pd, 3 at.% Cu and 44 at.% Sn for the voltammetric activated counterpart. Compared with the bulk composition of activated PdCuSn/CNTs (ca. 47.29 at.% Pd, 20.82 at.% Cu, 31.89 at.% Sn), it suggests that the voltage-sweeping may evoke an activated PdCuSn/CNTs catalyst with a PdSn-enriched shell, as illustrated in Fig. 11.

On one hand, the surface depletion of Cu from alloy nanocages and nanoparticles would actually result in surface roughing topography, as exemplified by several groups such as Xia et al. [69] and Strasser et al. [70–72]. More importantly, highly active PdSn bimetallic clusters would evolve on the superficial surface due to the leaching of neighboring Cu atoms. Prior to CV pretreatment, the XPS result shown in Fig. 10c indicates that the topmost Sn species on the PdCuSn/CNTs will exist in a mixture of Sn (0), Sn (II) and Sn (IV). However, the shifting of Sn 3d binding energy to high valence state indicates that the oxygen or hydroxyl radicals will be more prone to adsorb onto the low coordination Sn sites through activation process (depletion of Cu). Normally, the activity enhancement of electrocatalyst can be explained by bi-functional and/or electronic (ligand) effects [73,74]. Switzer et al. [36] and Wen et al. [75] also reported that, there exists a benefit of Sn/SnO_2 to platinum group metal catalyst for oxidation of small organic molecules and ascribe to the reason that the presence of oxophilic Sn species improves the capability to remove adsorbed CO. The facility of oxygen-containing species adsorbed onto the catalyst surface at lower potential is of great significance for the oxidation of carbonate intermediates and that is so-called bi-functional effect. In addition, except for the as-evolved core–shell characteristic, the leaching of less noble atoms would introduce a series of geometric changes on the surface of catalyst, such as strain, defects and/or dislocations, etc, which will further modify the surface atomic environment as well as the electronic structure [24,76]. Thus, it is reasonable that the highly enhanced activity of PdCuSn/CNTs surrounded by PdSn(O) shell derives from the mechanism that, on one hand, the adsorption of oxygen or hydroxyl radicals on Sn sites adjacent to the reacting species enhances the oxidation reaction of either the fuel or the poisoning intermediate. On the other hand, the distinct shell (PdSn(O)-rich)/core (base-metal-rich) characteristics are also likely to affect the electronic feature of Pd surface, thus modifying chemisorption energies of reaction intermediates and activation barriers of catalytic process. Of course, the in-depth reason should be further explored relying on more sophisticated instruments in the future work.

4. Conclusions

Mono-Pd/CNTs, binary PdCu/CNTs, PdSn/CNTs and ternary PdCuSn/CNTs catalysts have been synthesized by $NaBH_4$ reduction method. During the voltage-cycled activation, Cu is more prone to suffer leaching while the dissolution of Sn can rarely occur. For methanol oxidation, the promotion effect of Sn is comparable

with that of Cu. For ethanol and formic acid oxidation, however, the promotion effect of Sn is prominent. The PdCuSn/CNTs reveals the best activity toward methanol, ethanol and formic acid electrooxidation and the corresponding mass activity can attain to 395.94, 872.70 and 534.83 mA mg^{-1} Pd, respectively. The excellent activity of ternary PdCuSn/CNTs should be attributed to the bifunctional and electronic mechanism based upon the depletion of surface Cu atoms as well as widely-embedded PdSn(O) nanoclusters on the superficial surface.

Acknowledgments

The authors acknowledge financial support by National Natural Science Foundation of China (51201113, 51171125), National Basic Research Program of China (973, 2012CB932800), the 51st China Postdoctoral Science Foundation (2012M510781), Natural Science Youth Foundation of Shanxi Province (2013021011-4) and Taiyuan University of Technology Talents Fund (tyut-rc201115a).

References

[1] D. Chu, S. Gilman, J. Electrochem. Soc. 143 (1996) 1685–1690.
[2] S. Ha, Z. Dunbar, R.I. Masel, J. Power Sources 158 (2006) 129–136.
[3] C. Bianchini, P.K. Shen, Chem. Rev. 109 (2009) 4183–4206.
[4] L.L. Zhang, T.H. Lu, J.C. Bao, Y.W. Tang, C. Li, Electrochem. Commun. 8 (2006) 1625–1627.
[5] F. Maroun, F. Ozanam, O.M. Magnussen, R.J. Behm, Science 293 (2001) 1811–1814.
[6] A. Ruban, B. Hammer, P. Stoltze, H.L. Skriver, J.K. Nørskov, J. Mol. Catal. A Chem. 115 (1997) 421–429.
[7] F.L. Cheng, X.C. Dai, H. Wang, S.P. Jiang, M. Zhang, C.W. Xu, Electrochim. Acta 55 (2010) 2295–2298.
[8] S.T. Nguyen, H.M. Law, H.T. Nguyen, N. Kristian, S.Y. Wang, S.H. Chan, X. Wang, Appl. Catal. B 91 (2009) 507–515.
[9] A.O. Neto, M.M. Tusi, N.S.O. Polanco, S.G. Silva, M.C. Santos, E.V. Spinacé, Int. J. Hydrogen Energy 36 (2011) 10522–10526.
[10] Z.L. Liu, X.H. Zhang, L. Hong, Electrochem. Commun. 11 (2009) 925–928.
[11] Z. Qi, H.R. Geng, X.G. Wang, C.C. Zhao, H. Ji, C. Zhang, J.L. Xu, Z.H. Zhang, J. Power Sources 196 (2011) 5823–5828.
[12] D.M. Acosta, J.L. Garcia, L.A. Godinez, H.G. Rodríguez, L.Á. Contreras, L.G. Arriaga, J. Power Sources 195 (2010) 461–465.
[13] F.H.B. Lima, E.R. Gonzalez, Electrochim. Acta 53 (2008) 2963–2971.
[14] S.M.S.I. Dulal, M.S. Won, Y.B. Shim, J. Alloys Compd. 494 (2010) 463–467.
[15] T. Maiyalagan, K. Scott, J. Power Sources 195 (2010) 5246–5251.
[16] Y.C. Zhao, X.L. Yang, J.N. Tian, F.Y. Wang, L. Zhang, Int. J. Hydrogen Energy 35 (2010) 3249–3257.
[17] C.T. Hsieh, Y.W. Chou, W.Y. Chen, J. Alloys Compd. 466 (2008) 233–240.
[18] Y. Wang, Z.M. Sheng, H.B. Yang, S.P. Jiang, C.M. Li, Int. J. Hydrogen Energy 35 (2010) 10087–10093.
[19] Y. Wang, X. Wang, C.M. Li, Appl. Catal. B 99 (2010) 229–234.
[20] C.X. Xu, A.H. Liu, H.J. Qiu, Y.Q. Liu, Electrochem. Commun. 13 (2011) 766–769.
[21] Z.H. Zhang, C. Zhang, J.Z. Sun, T.Y. Kou, C.C. Zhao, RSC Adv. 2 (2012) 11820–11828.
[22] Z.L. Liu, X.H. Zhang, Electrochem. Commun. 11 (2009) 1667–1670.
[23] D.D. Tu, B. Wu, B.X. Wang, C. Deng, Y. Gao, Appl. Catal. B 103 (2011) 163–168.
[24] P. Strasser, S. Koh, T. Anniyev, J. Greeley, K. More, C.F. Yu, Z.C. Liu, S. Kaya, D. Nordlund, H. Ogasawara, M.F. Toney, A. Nilsson, Nat. Chem. 2 (2010) 454–460.
[25] M. Oezaslan, P. Strasser, J. Power Sources 196 (2011) 5240–5249.
[26] L. Gan, M. Heggen, S. Rudi, P. Strasser, Nano. Lett. 12 (2012) 5423–5430.
[27] P. Mani, R. Srivastava, P. Strasser, J. Power Sources 196 (2011) 666–673.
[28] K.C. Neyerlin, R. Srivastava, C.F. Yu, P. Strasser, J. Power Sources 186 (2009) 261–267.
[29] M. Oezaslan, F. Hasché, P. Strasser, J. Electrochem. Soc. 159 (2012) B444–B454.
[30] M. Oezaslan, F. Hasché, P. Strasser, J. Electrochem. Soc. 159 (2012) B394–B450.
[31] S.H. Yan, S.C. Zhang, Int. J. Hydrogen Energy 36 (2011) 13392–13397.
[32] Z.P. Sun, X.G. Zhang, Y.Y. Liang, H.L. Li, J. Power Sources 191 (2009) 366–370.
[33] C.H. Lu, L.M. Qi, J.H. Yang, D.Y. Zhang, N.Z. Wu, J.M. Ma, J. Phys. Chem. C 108 (2004) 17825–17831.
[34] G.H. Du, G.V. Tendeloo, Chem. Phys. Lett. 393 (2004) 64–69.
[35] Y. Wang, T.S. Nguyen, X.W. Liu, X. Wang, J. Power Sources 195 (2010) 2619–2622.
[36] E.E. Switzer, T.S. Olson, A.K. Datye, P. Atanassov, M.R. Hibbs, C.J. Cornelius, Electrochim. Acta 54 (2009) 989–995.
[37] M. Cheng, Z.B. Wang, Y. Ding, G.P. Yin, Electrochem. Commun. 10 (2008) 443–446.
[38] F. Colmati, E. Antolini, E.R. Gonzalez, J. Alloys Compd. 456 (2008) 264–270.
[39] B. Xue, P. Chen, Q. Hong, J.Y. Lin, K.L. Tan, J. Mater. Chem. 11 (2001) 2378–2381.
[40] S. Tominaka, Y. Nakamura, T. Osaka, J. Power Sources 195 (2010) 1054–1058.
[41] C.W. Liu, Y.W. Chang, Y.C. Wei, K.W. Wang, Electrochim. Acta 56 (2011) 2574–2581.
[42] X.Z. Xue, J.J. Ge, C.P. Liu, W. Xing, T.H. Lu, Electrochem. Commun. 8 (2006) 1280–1286.
[43] X.G. Wang, W.M. Wang, Z. Qi, C.C. Zhao, H. Ji, Z.H. Zhang, Electrochem. Commun. 11 (2009) 1896–1899.
[44] W. Pan, X.K. Zhang, H.Y. Ma, J.T. Zhang, J. Phys. Chem. C 112 (2008) 2456–2461.
[45] P. Strasser, S. Koh, J. Greeley, Phys. Chem. Chem. Phys. 10 (2008) 3670–3683.
[46] S. Koh, P. Strasser, J. Am. Chem. Soc. 129 (2007) 12624–12625.
[47] S. Koh, N. Hahn, C.F. Yu, P. Strasser, J. Electrochem. Soc. 155 (2008) B1281–B1288.
[48] P. Mani, R. Srivastava, P. Strasser, J. Phys. Chem. C 112 (2008) 2770–2778.
[49] S. Trasatti, O.A. Petrii, Pure Appl. Chem. 63 (1991) 711–734.
[50] Y.C. Zhao, L. Zhan, J.N. Tian, S.L. Nie, Z. Ning, Int. J. Hydrogen Energy 35 (2010) 10522–10526.
[51] M.H. Shao, K. Shoemaker, A. Peles, K. Kaneko, L. Protsailo, J. Am. Chem. Soc. 132 (2010) 9253–9255.
[52] C.H. Cui, H.H. Li, X.J. Liu, M.R. Gao, S.H. Yu, ACS Catal. 2 (2012) 916–924.
[53] S.S. Mahapatra, A. Dutta, J. Datta, Int. J. Hydrogen Energy 36 (2011) 14873–14883.
[54] R. Manoharan, J. Prabhuram, J. Power Sources 96 (2001) 220–225.
[55] Y.H. Qin, H.H. Yang, X.S. Zhang, P. Li, C.A. Ma, Int. J. Hydrogen Energy 35 (2010) 7667–7674.
[56] S.S. Mahapatra, A. Dutta, J. Datta, Electrochim. Acta 55 (2010) 9097–9104.
[57] Z.P. Sun, X.G. Zhang, R.L. Liu, Y.Y. Liang, H.L. Li, J. Power Sources 185 (2008) 801–806.
[58] X.G. Wang, W.M. Wang, Z. Qi, C.C. Zhao, H. Ji, Z.H. Zhang, J. Alloys Compd. 508 (2010) 463–470.
[59] C.W. Xu, Y.L. Liu, D.S. Yuan, Int. J. Electrochem. Sci. 2 (2007) 674–680.
[60] Y.W. Lee, S.B. Han, K.W. Park, Electrochem. Commun. 11 (2009) 1968–1971.
[61] F. Hu, F. Ding, S. Song, P.K. Shen, J. Power Sources 163 (2006) 415–419.
[62] L.D. Zhu, T.S. Zhao, J.B. Xu, Z.X. Liang, J. Power Sources 187 (2009) 80–84.
[63] X.G. Wang, W.M. Wang, Z. Qi, C.C. Zhao, H. Ji, Z.H. Zhang, Int. J. Hydrogen Energy 37 (2012) 2579–2587.
[64] E.C. Rivera, D.J. Volpe, L. Alden, C. Lind, C. Downie, T.V. Alvarez, A.C.D. Angelo, F.J. Disalvo, H.D. Abruña, J. Am. Chem. Soc. 126 (2004) 4043–4049.
[65] R.S. Jayashree, J.S. Spendelow, J. Yeom, C. Rastogi, M.A. Shannon, P.J.A. Kenis, Electrochim. Acta 50 (2005) 4674–4682.
[66] Q.F. Yi, W. Huang, X.P. Liu, G.R. Xu, Z.H. Zhou, A.C. Chen, J. Electroanal. Chem. 619–620 (2008) 197–205.
[67] S. Ha, R. Larsen, Y. Zhu, R.I. Masel, Fuel Cells 4 (2004) 337–343.
[68] S. Ha, R. Larsen, R.I. Masel, J. Power Sources 144 (2005) 28–34.
[69] B.Y. Xia, H.B. Wu, X. Wang, X.W. Lou, J. Am. Chem. Soc. 134 (2012) 13934–13937.
[70] C.H. Cui, L. Gan, H.H. Li, S.H. Yu, M. Heggen, P. Strasser, Nano. Lett. 12 (2012) 5885–5889.
[71] L. Gan, M. Heggen, R. O'Malley, B. Theobald, P. Strasser, Nano. Lett. 13 (2013) 1131–1138.
[72] M. Oezaslan, M. Heggen, P. Strasser, J. Am. Chem. Soc. 134 (2012) 514–524.
[73] M. Watanabe, S. Motoo, J. Electroanal. Chem. 60 (1975) 259–266.
[74] B. Hammer, J.K. Nørskov, Surf. Sci. 343 (1995) 211–220.
[75] Z.L. Wen, S.D. Yang, Y.Y. Liang, W. He, H. Tong, L. Hao, X.G. Zhang, Q.J. Song, Electrochim. Acta 56 (2010) 139–144.
[76] L. Gan, R. Yu, Z.Y. Cheng, J. Zhu, J. Phys. Chem. Lett. 3 (2012) 934–938.